

New Approaches for the Manufacturing and Characterization of Smart Structures made of Fiber-Reinforced Plastics

B.Kelkel^{*}, R. Sebastian^{*}, M. Hübler^{*}, M. Gurka^{*}

^{*}Institut für Verbundwerkstoffe GmbH

Erwin-Schrödinger-Straße

67663 Kaiserslautern

Benjamin.kelkel@ivw.uni-kl.de

ron.sebastian@ivw.uni-kl.de, moritz.huebler@ivw.uni-kl.de, martin.gurka@ivw.uni-kl.de

Key words: shape memory alloy, shape control, piezoelectric transducer, structural health monitoring, guided waves

Summary:

This work deals with the manufacturing and characterization of smart structures made of fiber-reinforced plastics (FRP) and active elements like shape memory alloy (SMA) wires or piezoelectric transducers. Manufacturing processes for the structural integration of these elements as well as methods for their characterization are presented.

Active elements like SMA wires and piezoelectric transducers enable new functionalities in various areas of application. SMA wires show outstanding actuation performance (up to 6% strain) that allow for active shape change in aircraft wings, air inlet vents or car spoilers. On the other hand, piezoelectric transducers are highly sensitive to acoustic waves and therefore suitable for non-destructive testing and the realization of sensor networks for guided wave structural health monitoring (SHM) systems. However, the lack of robust manufacturing processes that offer easy and repeatable integration of active elements and the deficiency of applicable characterization methods that facilitate the design of active components, impede the breakthrough of these smart structures.

These circumstances are the starting point for this study which promotes the development of modular manufacturing methods which do not only feature reproducibility and robustness but also are applicable to conventional FRP production processes (RTM, Autoclave). A common challenge in the manufacturing of smart structures is the assurance of adequate mechanical coupling without the deterioration of the mechanical properties of the structure. The study investigates this challenge and proposes methods for the optimization of the interface in terms of load transfer and acoustic coupling respectively. A standardized, modular concept for the integration of active elements in various fiber-reinforced plastics is finally presented as an outlook.

Besides the new manufacturing concepts, the study proposes standardized testing methods for describing not only the active element itself but also the smart structure as a whole. Concerning SMA, a method for the determination of maximum deflection and stress as a function of structure stiffness is presented. Regarding the realization of SHM systems, a closer look is taken at the dispersion and attenuation of guided waves in FRP.

1 INTRODUCTION

Increasing functional integration within technical products is seen to enable substantial savings. Fiber-reinforced composites allow for easy integration of sensors or actuators into structural components, which turns these materials into active structures, also called smart structures or smart materials [1]. High performance composite materials are already used in a wide range of applications and their share is still increasing, as demonstrated by the latest aircrafts of leading manufacturers incorporating more than 50 % composite materials [2].

FRP combine the advantages of a polymer matrix and reinforcing fibers to superior properties of the composite. This inherent modular character enables various possibilities for the integration of active elements. Similar to the fiber integration in FRP, orientation and content of active elements in the composite can be defined individually and tailored for efficiency. A wide range of multifunctional materials is available (e.g. piezoelectric materials, magnetostrictive materials, shape memory alloys) that show unique behavior and can be used for special applications [1].

In the field of solid-state actuators, shape memory alloys (SMA) show an outstanding performance. They reach high actuation travel and stress levels at the same time, leading to a high volumetric energy density.

For shape control purposes, SMA offers an actuation capability with a strain of up to 6 % and a stress of up to 600 MPa. This performance matches the mechanical behavior of FRP. By the use of SMA wires, a high degree of adaptability of the active elements can be achieved.

The memory effect is based on the transition between the low temperature martensite phase and the high temperature austenite phase. Newly formed martensites have a twinned microstructure: Deformation leads to a detwinning of the material, allowing for the introduction of a high amount of remanent strain, similar to a plastic deformation. Heating above the austenite start temperature AS initiates the phase transition to the austenitic phase. At the austenite finish temperature AF the material finally restores its original shape. This contraction can be used for actuation. The effect, described and shown in Figure 1 a), is the so called one-way effect. The sample remembers only the geometry in the austenite phase. The other shape memory effect, which can be obtained by a special training process, is the two-way-effect. In this case, the specimen remembers a specific shape for both phases (see Figure 1 b).

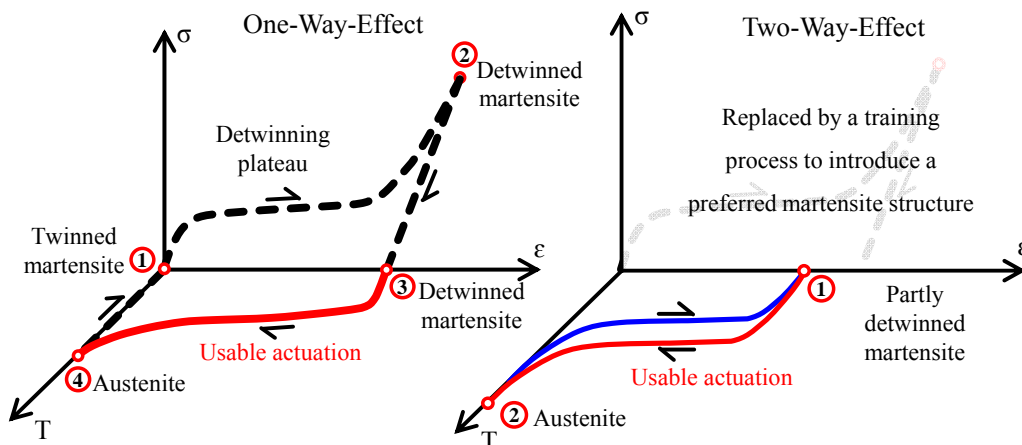


Figure 1: One-Way Effect and trained Two-Way Effect of Shape Memory Alloys.

Even though there is a two-way effect seen in this investigation, it is necessary to differentiate between the above-mentioned ‘trained’ two-way effect and the later shown load-initiated two-way effect. The ‘trained’ two-way effect can only be obtained after the time-consuming cycling of the material. Alternatively, two one-way effect elements can be mechanically combined in a system, working against each other, thus creating a two-way actuator [3]. In contrast, the load-initiated two-way effect offers a cheap way to gain this two-way functionality [4].

Even though the effect is temperature driven, the forward transition to austenite and the actuation can be achieved on-demand even for integrated elements by a simple joule heating. If necessary, the activation can be initiated within a split second by joule heating [5].

In principle the integration of SMA wires is feasible in many ways; however, the load transfer from the high performance actuator wires to the FRP structure is a major challenge. Current approaches for SMA/FRP composites [6-9] are based on the integration of individual SMA elements with free ends assuming sufficient shear strength of the SMA-FRP-interface for the load transfer during actuation.

Piezoelectric materials can act as sensors or actuators through the piezoelectric effect that enables the conversion of electric to mechanical energy and vice versa. The direct piezoelectric effect describes the generation of an electric charge upon mechanical straining of the piezoelectric material (sensor effect). This effect is reversible and leads to the inverse piezoelectric effect which facilitates the generation of mechanical strain through the application of an electric field to the piezoelectric material (actuator effect). Both effects occur simultaneously in ceramics, exhibiting a non-centrosymmetric perovskite structure (e.g. barium titanate or lead zirconium titanate), in crystals (e.g. quartz or tourmaline) as well as in certain polymers (e.g. PVDF - polyvinylidene fluoride). Relevant piezoelectric materials for industrial use are ceramics like barium titanate and lead zirconium titanate. These ceramics exhibit large piezoelectric coefficients, leading to an efficient electromechanical coupling.

Due to their sensitivity and fast response characteristic, piezoelectric materials can be utilized for the excitation and detection of ultrasonic waves in Structural Health Monitoring (SHM) applications. In the form of discs or patches, piezoelectric sensors/actuators can be integrated into FRP structures to allow for an active or passive monitoring [10]. In the case of passive monitoring systems, piezoelectric transducers act as sensors that detect acoustic emissions from the initiation and development of material flaws (e.g. cracks or delaminations). In contrast, active systems utilize piezoelectric transducers to sense and excite ultrasonic waves in order to detect their interaction with present flaws in the material. In thin plate-like structures these waves propagate in the form of guided waves (Lamb waves) which are dispersive by nature and occur in symmetric and asymmetric modes. Due to their high sensitivity to flaws (e.g. delaminations) and their moderate attenuation in FRP, Lamb waves became of growing interest for the realization of SHM systems in FRP [11]. In this context, the characterization of Lamb wave propagation (dispersion and attenuation) is of substantial interest for the design and the reliability of a SHM system.

This study is focused on SMA wires and piezoelectric transducers as actuating and sensing elements in FRP. For a clear arrangement, both types of functional elements are discussed separately throughout the paper. At the beginning, manufacturing methods for the integration of SMA wires and piezoelectric transducers are presented with a discussion on the major challenges. Afterwards, methods for the characterization of SMA actuated structures and guided wave SHM systems are described.

2 MANUFACTURING METHODS

2.1 Integration of SMA wires

SMA wires cannot be integrated into FRP the same way as the reinforcing fibers because common SMA elements have a significant higher diameter, which considerably affects the load transfer. Additionally, a current supply for each wire has to be granted.

This results in major drawbacks:

- Potential interface failure between SMA and FRP
- Extensive current connections waste space and add weight
- Reproducibility is critical concerning a precise alignment during manufacture; especially with a higher number of smaller SMA elements, extensive rigs are necessary.

A new concept has to provide sufficient solutions for all these challenges. While the problem regarding the electrical connection and the reproducibility during manufacturing is obvious, the challenge of ensuring sufficient load transfer requires a closer look. Due to market availability and easy handling during manufacturing, a minimum diameter for the SMA elements is recommended. Any deformation of the wire leads to a shear stress that is being transferred through the interface of the SMA wire and the surrounding FRP matrix. Since the wire is of finite length, there is a highly localized shear stress at its free ends, impeding the already challenging situation. The maximum shear stress depends on the elastic properties of the materials and many other parameters [12].

The concept presented in Figure 2 is based on the idea of utilizing material interlocking between active SMA wires and passive anchor wires. The prepared semi-finished SMA grid has an anchoring wire welded to the active wires. This supports stiffness and strength and enables electrical contacting at the same time. A well designed semi-finished SMA grid, as presented in Figure 2, provides solutions for all mentioned challenges, if the following assumptions are taken into account:

- The anchoring cross-wire does not show any actuation by heating
- The cross-section of the anchoring wire is similar to the sum of the cross-sections of all the wires connected in parallel
- Local reinforcements at the anchoring wire are provided by the FRP part, in order to support the load transfer

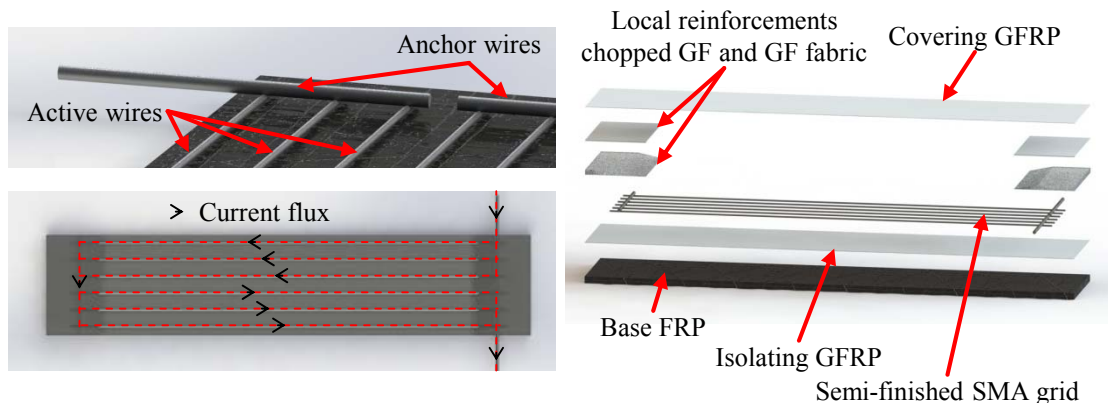


Figure 2: Integration concept using a semi-finished SMA grid.

The semi-finished grid improves the handling during manufacturing; in consequence a better alignment is ensured. The required electrical network is formed by the anchor wires as well. For 6 active SMA wires originally 12 electrical connection elements were necessary, whereas in the new design only two electrical contacts are supplying the entire structure.

By means of the anchor wires the loading situation is changed from interface shear to surface pressure. Therefore, local reinforcements in the form of chopped glass fibers and glass fiber fabrics are added on top of the FRP. The cross sections, presented in Figure 3, show a promising result with a significant welding zone and fibers in place for a proper load transfer.

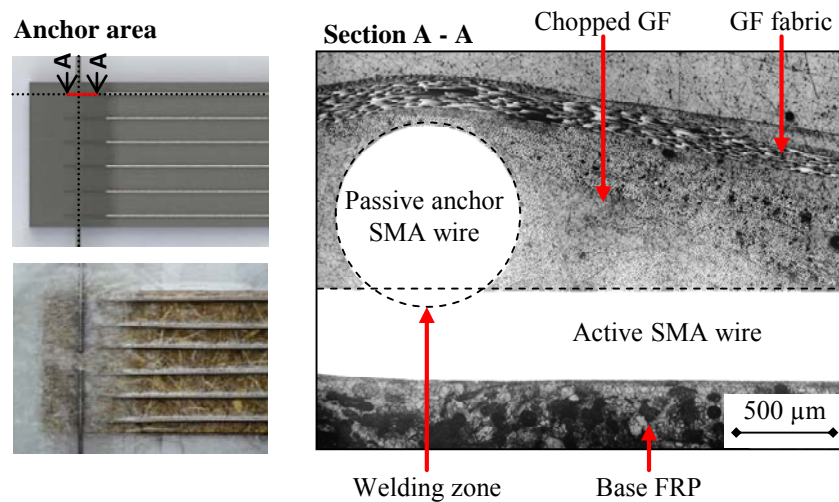


Figure 3: Sections of anchor area with welding zone and reinforcing fibers.

2.2 Integration of piezoelectric transducers

A method for the integration of piezoelectric transducers has to account for a proper connection of sensors. Commonly available sensor types are piezoelectric wafer active sensors (PWAS), piezoelectric patch transducers and macro fiber composites (MFC). The integration of these sensors is usually done in a post-process by secondary bonding. In order to be successful, this process has to be well-conditioned, assuring clean surfaces, optimal process parameters and protection against environmental influences. For the evaluation of bonding quality, additional non-destructive testing methods have to be applied. This results in a time consuming and sensitive process which lacks reproducibility. Regarding the modular character of FRP, a direct integration of sensors can be achieved within the original manufacturing process. This way, a primary bond between sensor and substrate can be achieved in one step, omitting the post-process for secondary bonding. Furthermore, sensor and wiring can be supplied as an integrative component (sensor unit) directly to the manufacturing process to simplify the handling and support reproducibility.

This approach of direct sensor integration was followed in this study. The resin transfer molding (RTM) process was chosen as the targeting manufacturing process. During this manufacturing process dry preformed fabrics are stacked in a mold and are subsequently infiltrated by resin under high pressure [13].

For the integration of piezoelectric sensors during the RTM process, a custom mold was designed and manufactured. The mold allows for the production of flat panels (250 x 200 mm) with integrated sensor units. A schematic overview of this unit within the mold can be seen in Figure 4.

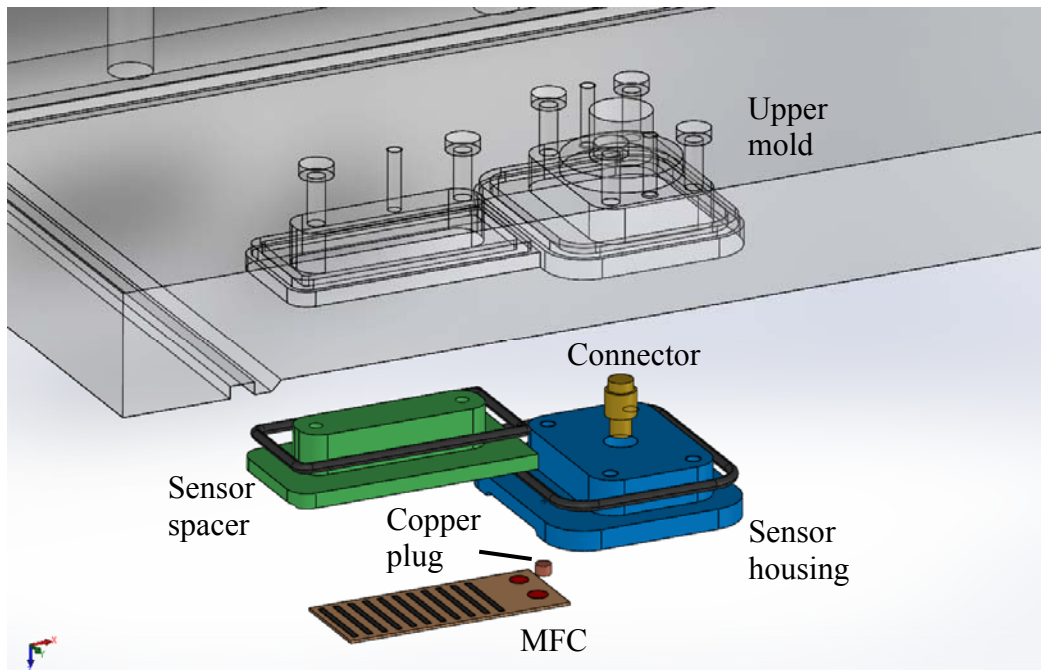


Figure 4: Schematic overview of the sensor unit.

The unit consists of a MFC sensor, a connector, a sensor spacer and housing. For convenient processing the ground of the MFC is soldered to a copper plug which is part of the sensor housing. The MFC is additionally bonded to the sensor spacer with conventional epoxy in order to guarantee the sensor position during processing. Signal line connection between sensor and connector is realized by conventional wiring. The sensor unit can be supplied as a complete assembly to the upper mold. Interchangeability between sensor types is given by the sensor spacer that can be adjusted according to the geometry of the sensor. In order to protect the connector from the resin, the insert is sealed.

Figure 5 shows the upper part of the mold with the inserted sensor unit.

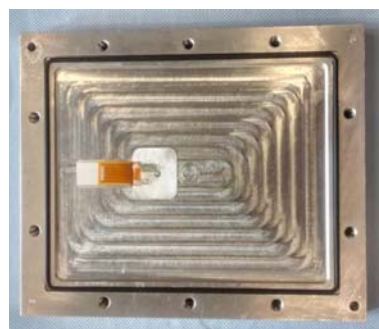


Figure 5: Upper mold with integrated sensor unit.

MFC sensors of type M2814-P1 (Smart Material GmbH, Germany) were chosen. The panels were built up from a quasi-isotropic layup of conventional carbon fiber woven fabrics and epoxy. The finished panel with integrated sensor unit is shown in Figure 6.



Figure 6: Finished panel with integrated sensor unit.

Since the sensor is attached to the structure within the original manufacturing process, a primary bonding takes place which supports reproducible signal integrity. Signal quality was characterized using a HSU-Nielsen source. Compared to secondary bonded MFCs, an improvement in signal to noise ratio could be observed, indicating the ability of detecting acoustic emissions with the integrated sensor.

3 CHARACTERIZATION METHODS

Characterization is crucial for an efficient and reliable design of smart structures. For the development of characterization methods, a closer look is taken at the constitution of smart structures first.

Smart structures can be seen as systems that consist of several sub systems (interfaces, active elements, substrate, etc.) that interact with each other. The function of these sub systems is to guarantee energy transfer between the central active element and the system boundaries. Energy enters a sub system, is converted and transferred to the next system. A functional analysis can give insights in the system architecture and the energy flow between the components.

The energy conversion and transfer can be achieved by various physical effects (Joule heating, piezoelectric effect, shape memory effect) that are governed by different functional properties (specific resistivity, piezoelectric charge constant, transition temperature). In order to describe the reaction of a smart structure to an external stimulus, these functional properties have to be identified and determined by applicable characterization methods.

In some cases, isolation of certain sub systems for characterization is not possible. Here, characterization methods have to be developed that are able to separate the effect of certain sub systems within a system.

The following sections investigate these circumstances and elaborate on the characterization of SMA- and guided wave SHM systems in particular. Exemplary methods for the determination of functional properties are presented and discussed.

3.1 Characterization of SMA actuated structures

As discussed before, not all sub systems can be characterized individually. While the generation of thermal energy via Joule Heating of SMA elements is more or less independent of the other systems, the shape memory effect is heavily affected by the behavior of the counterpart. The interface is in charge of the load transfer and has to be capable of withstanding the present stresses. The interaction of sub systems is demonstrated in Figure 7 using a simplified functional analysis. Caused by the strong influence of the external load on the shape memory effect, the characterization takes two sub systems into account: the SMA- and the counter acting substrate system. Therefore, the characterization of the actuator performance was done in a configuration, where the SMA-actuator is working against a defined spring-stiffness, which represents the elastic response of the FRP structure. Via a variation of the spring rate, different load cases can be simulated

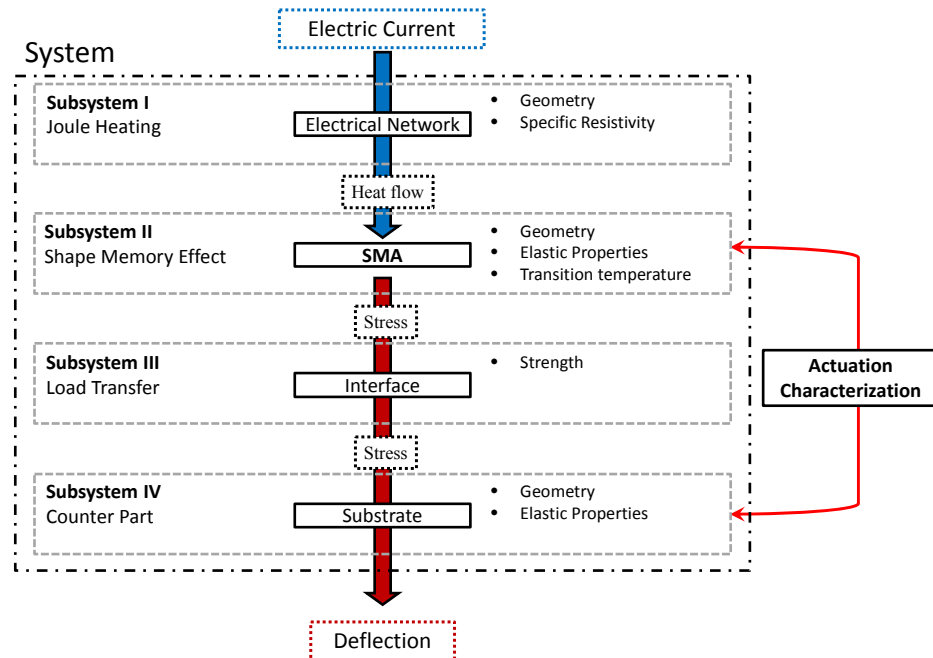


Figure 7: Functional analysis of active SMA FRP hybrid structures.

Experimental Setup

A schematic setup for the realization of the relevant load case is shown in Figure 8. Due to the more linear characteristic, compression springs are used instead of tension springs. The springs are mounted to a special housing that facilitates the load transfer between the SMA wire and the spring. The SMA wire is held in place by the clampings which also enable the electrical connection. Measurement of elongation was done using macro displacement transducers, located directly at the spring housing to ensure the measurement of the complete strain of the SMA wire. Furthermore, the temperature was measured by a thermocouple. To activate the actuation, the pre-strained wires are heated up via Joule Heating with 8 A up to 120°C.

A one-way-effect material, Alloy M (Memry Corporation, USA), with a diameter of 1 mm was used for the test. Before the actual test, the SMA wires were heated up to 100°C, well above the activation temperature, to remove all prior deformation. After cooling down to

room temperature, a well-defined pre-strain was introduced, using a universal tensile testing machine with a free length similar to the length used for the actual characterization. The pre-straining process was carried out with a speed of 250%/min to ensure a homogenous strain distribution [14]. The pre-strain values were adjusted to 1.8%, 3%, 4.5% and 6.3%.

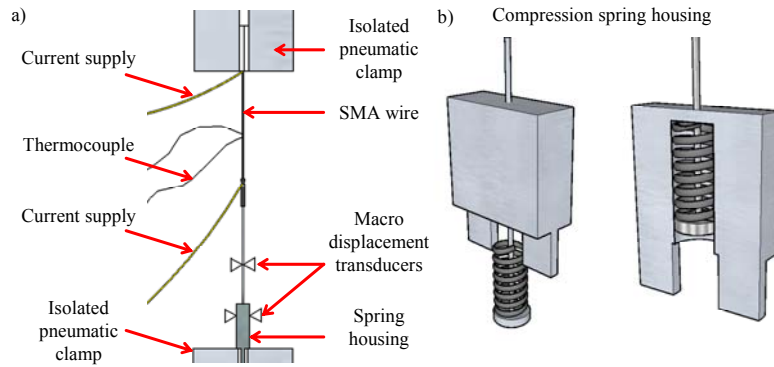


Figure 8: Test setup to characterize the SMA wire working against a spring stiffness.

Results

The result of a single test is shown in Figure 9. Exemplarily depicted are the pre-straining and 3 actuation cycles of a single wire working against a defined stiffness. The first heating (point 1 to 2) shows the highest contraction value. Afterwards a load-initiated elongation takes place (point 2 to 3), but the original shape is not recovered completely as the one-way-effect material has no intrinsic stimulus to recover the original shape. The change in strain which takes place during the cool down can be retrieved in subsequent heating cycles (point 3 to 2), indicating a load-initiated two-way actuation. In Figure 9 b) the strain over temperature for the same test is shown. The first contraction starts at about 35°C and is finished at about 50°C. With further heating, only the common thermal expansion can be observed, since the shape memory effect is already completely exploited at 50°C for this special load case. The mentioned load-initiated two-way effect takes place in a narrower temperature range, starting at 35°C and finishing at 40°C.

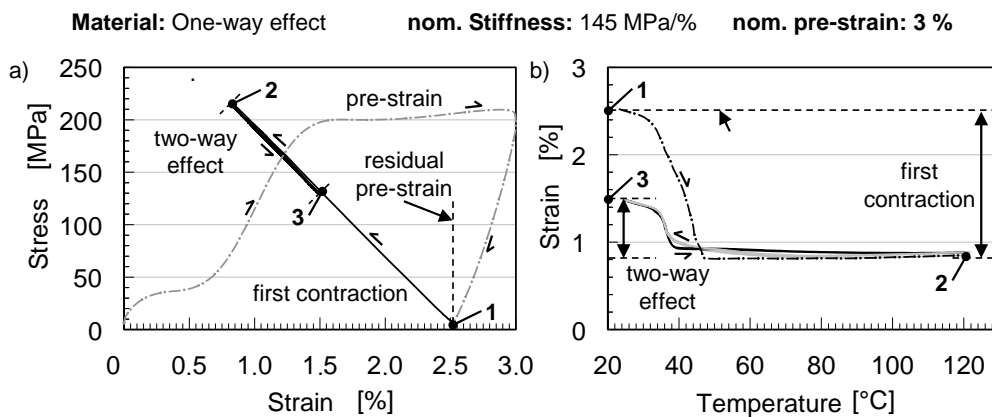


Figure 9: Result of an actuation test of a one-way effect SMA wire showing a load-initiated two-way effect.

As described before, the actuation of a single SMA strongly depends on the loading situation. How stiffness affects actuation can be seen in Figure 10. Tailoring the actuation travel by a well-defined pre-straining of the SMA material is an interesting option for many applications.

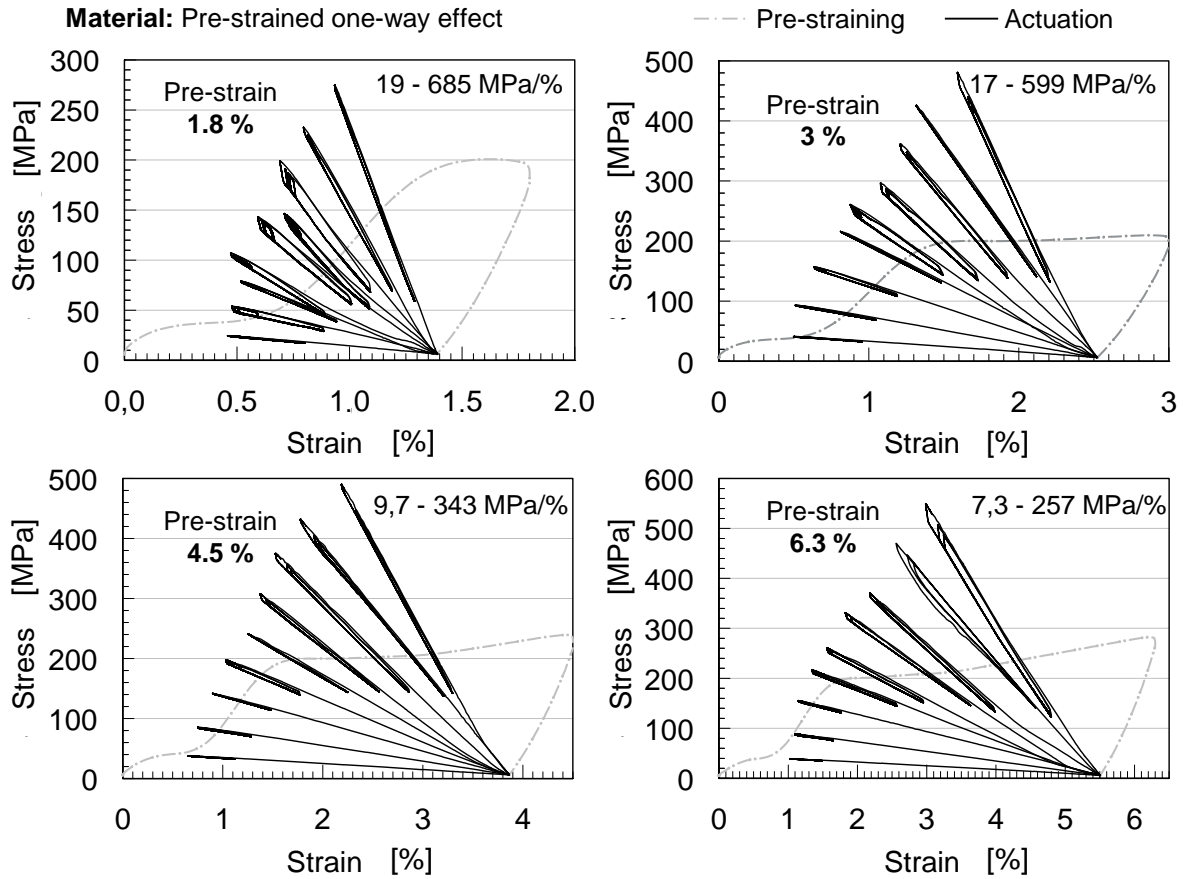


Figure 10: Actuation behavior of a one-way effect material with different pre-strain values working against a wide range of stiffnesses.

An impressive performance with 3.5% contraction at a stress level above 300 MPa can be achieved, when the sample was pre-strained up to 6.3%. At the same time, the load initiated two-way-effect shows a value of about 2%. The results built up a comprehensive data base that enables the description of SMA actuated structures. Using the data as input for a finite element analysis allows the simulation of the structure where the influence of counterpart stiffness on the shape memory effect is taken into account.

3.2 Characterization of guided wave SHM systems

The hardware side of a guided wave SHM system can be built up from an actuator, a coupling media, a substrate and a sensor. Their interaction is shown in form of a functional model in Figure 11.

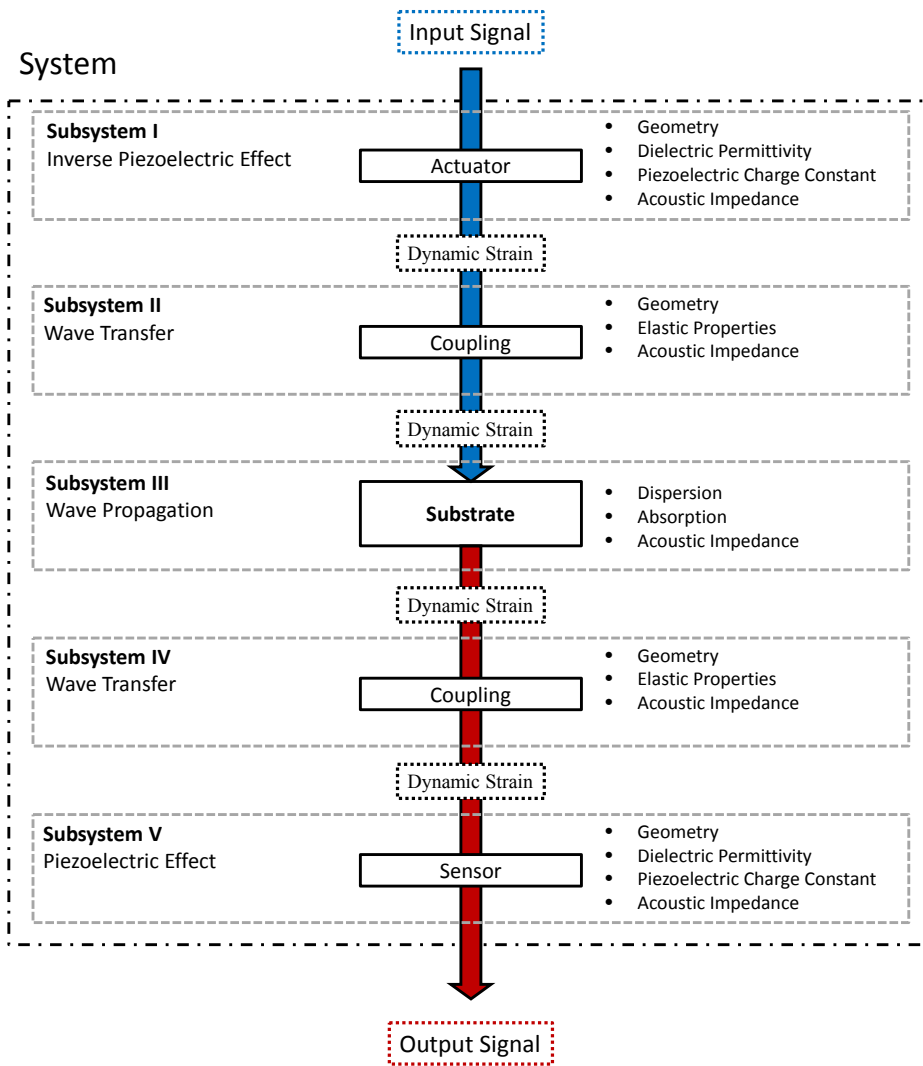


Figure 11: Functional analysis of a guided wave SHM system.

Whereas actuator and sensor are responsible for the initiation and detection of elastic waves, the coupling media and the substrate serve as wave guides. As already mentioned, functionality of sensor and actuator is governed by its geometry, dielectric permittivity and piezoelectric charge constant. Regarding the substrate, the characterization has to focus on material absorption and dispersion characteristics. However, not all parameters differ between systems. A common functional parameter between all sub systems is the acoustic impedance which governs the wave transfer throughout the entire system. This internal dependency impedes the characterization of single sub systems and thereby the separation of sub system influences. Characterization methods have to account for this instance by keeping side effects of sub systems manageable.

This study faces these circumstances and takes a closer look at the characterization of wave propagation within the substrate, suggesting a method for the determination of dispersion and attenuation of guided waves in carbon fiber-reinforced plastics.

Experimental Setup

The Experimental setup for the determination of Lamb wave dispersion and attenuation characteristics in thin walled FRP structures is shown in Figure 12. The central element is the NI PXIe 1062 Q system which enables direct communication between hard- and software components. The system is equipped with the following components:

- Arbitrary Waveform Generator (NI PXI-5422) - 200 MS/s, 16-Bit
- 8-Channel Oscilloscope/Digitizer (NI PXI-5105) - 60 MS/s, 12-Bit
- DAQ Module (NI PXI-6221) - 250 kS/s, 16-Bit

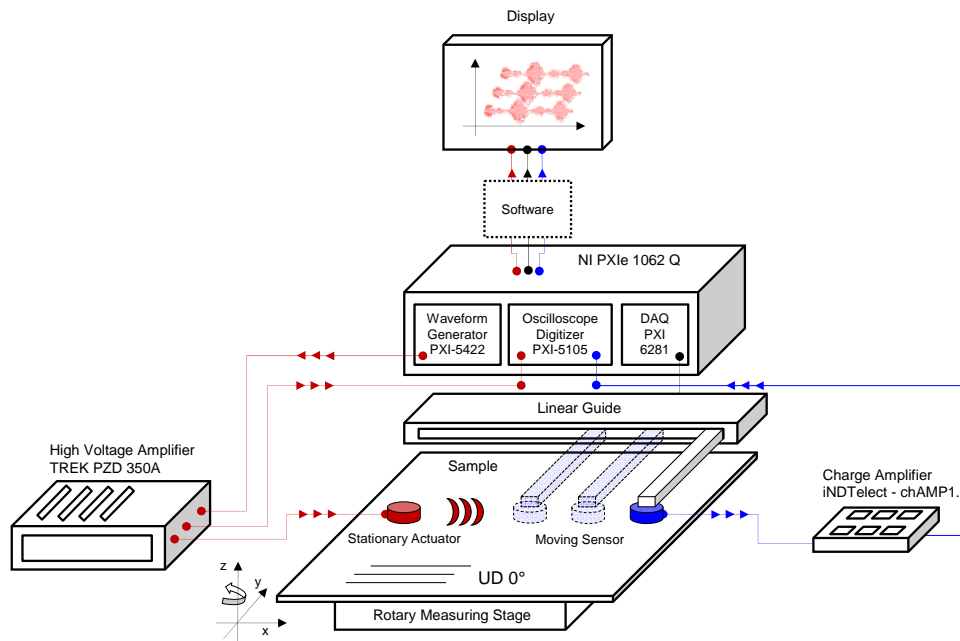


Figure 12: Experimental Setup for the determination of Lamb wave dispersion and attenuation.

Testing was performed on a composite panel built up of 8-ply SigrateX Prepreg CE 1007-150-38 (SGL Group, Germany) unidirectional carbon fiber with the layup $(0)_{4s}$. The sample was vacuum bagged and cured in an autoclave at 130°C and 24 bar for 60 minutes, resulting in a thickness of 1.15 ± 0.05 mm. After curing, the panel was cut to the dimensions 300×300 mm.

The panel is placed on a rotary measuring stage which allows for manual adjustment ($\pm 1^{\circ}$) of panel orientation in the x-y plane. This way, the anisotropic properties of CFRP can be visualized regarding Lamb wave propagation.

Lamb wave excitation and sensing is realized by two VS150-M (Vallen Systems GmbH, Germany) transducers that are placed 30 mm apart at the beginning of the measurement cycle. The cylindrical shaped transducers (diameter 20.3 mm) show a high sensitivity in the frequency range of 100 – 450 kHz with a resonance at 150 kHz. Coupling is achieved via silicon high vacuum grease (Losimol GmbH, Germany) on the actuator side and via water at the sensor side. The sensor is attached to a linear guide (isel Germany AG, Germany) that is driven by a micro-stepper motor and controlled via LabView and the DAQ module. Sensor positioning can be realized in steps of $2.5 \mu\text{m}$ from 30 to 300 mm. Due to limited plate

dimensions, the measuring range was set from 30 to 100 mm. An appropriate step size of 1 mm was chosen for all cycles.

The input signal from the arbitrary waveform generator was chosen as a five cycle tone burst modified by a Hanning window function. The frequency of the tone burst was varied between 100 kHz and 400 kHz in steps of 100 kHz for each sensor position. The time between subsequent bursts was set to 1.2 s in order to avoid interference between signals. Prior to sensor excitation the signal was amplified by the high voltage amplifier PZD350A (TREK INC., USA) with a maximum achievable gain of 150V/V. The gain was varied between cycles for optimum signal to noise ratio (SNR) without overloading the charge amplifier. Charge conversion and amplification was realized via the charge amplifier iNDTelect chAMP 1.1 (iNDTact GmbH, Germany) that enables high pass filtering and gradual amplification between -40 and 40dB in steps of 20dB. Amplification was set to 40 dB and a high pass filter was set up to reduce the level of noise.

Generator and sensor signals are tracked and digitized with a sample rate of 3 MS/s by the Oscilloscope/Digitizer. The selection of 4000 samples resulted in a cycle time of 1330 μ s. Prior to displaying, the digitized signals are filtered in the time domain with a first order Butterworth band-pass. The filter was set up around the frequency of the generator signal with a tolerance of ± 10 kHz in the frequency range.

An example for a generator and a corresponding sensor signal can be seen in Figure 13 for the investigated composite plate. Frequency of input signal was set to 275 kHz.

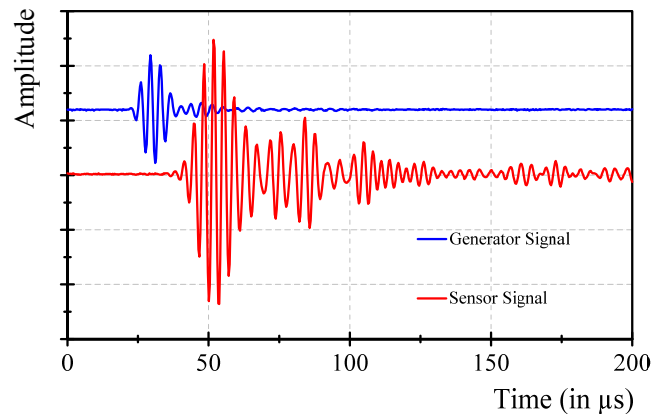


Figure 13: Input signal and corresponding output signal in 90° direction at a generator frequency of 275 kHz.

Data Analysis

For demonstration purposes, the data analysis is presented for a test series in the 90° direction in the following (perpendicular to the direction of fibers). For Lamb wave visualization, the signal amplitudes are displayed with respect to time and space in a colour coded 2D plot. The values are interpolated in between sampling points. An example can be seen in Figure 14 for a generator frequency of 275 kHz in the 90° direction.

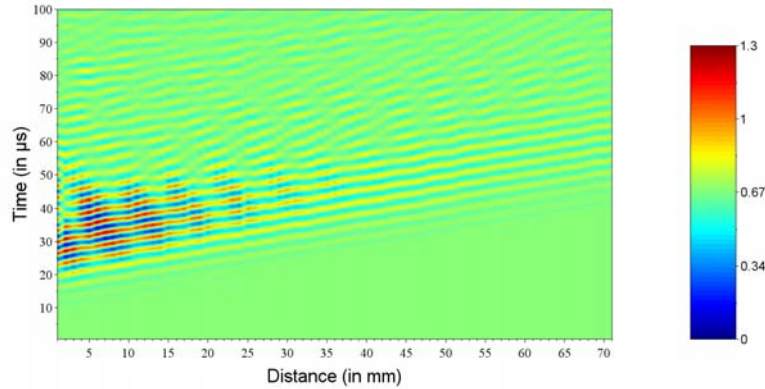


Figure 14: Colour coded 2D plot of signal amplitude (in mV) over time (in μs) and distance (in mm) at a generator frequency of 275 kHz in the 90° direction.

For the identification of Lamb wave modes a 2D-Fast Fourier Transformation (FFT) [15] was applied to the data, revealing information on dominant frequencies in time and space. Figure 15 shows the result of this transformation for the data in Figure 14.

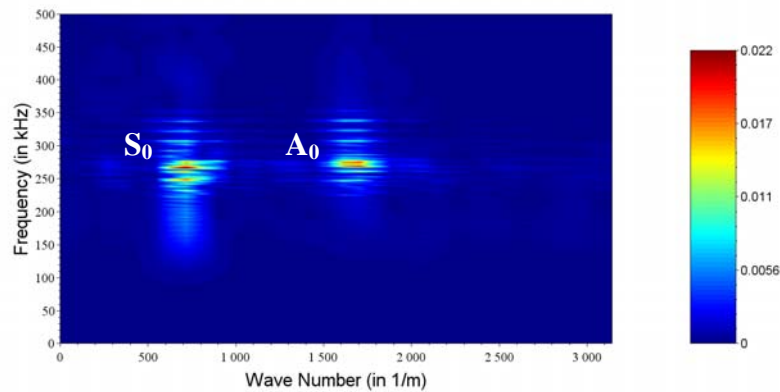


Figure 15: 2D-Fast Fourier Transformation of Figure 14 (Generator frequency 275 kHz, 90° direction).

Peaks in the 2D-FFT refer to either single Lamb wave modes or superpositions of them, whereby the peak coordinates represent the corresponding frequency f and wave number k . Two peaks can be identified in Figure 14, referring to the fundamental symmetric (S_0) and asymmetric (A_0) mode respectively. With the relationship

$$c_{ph} = \frac{2\pi}{k} \cdot f \quad (1)$$

the resulting phase velocities c_{ph} of both modes can be calculated. Table 1 summarizes the results.

Parameter/Mode	A_0	S_0
Frequency (in kHz)	275	275
Wave number (m^{-1})	1700	720
Phase velocity (in m/s)	1016	2400

Table 1: Frequencies, wave numbers and resulting phase velocities of A_0 and S_0 mode at a generator frequency of 275 kHz in the 90° direction. Results are obtained from the 2D-FFT in Figure 15.

For a separation of identified Lamb wave modes an additional band-pass filter was applied in space domain. A third order Butterworth filter was set up around the respective wavelength of present wave modes. Figure 16 and Figure 17 show the results that were achieved by applying two single band-pass filters according to Table 2 to the original data in Figure 14. This representation allows for an individual and independent analysis of wave modes.

Parameter/Mode	A_0	S_0
Lower wave number limit (in m^{-1})	1580	565
Upper wave number limit (in m^{-1})	1820	880

Table 2: Limits for the the third order Butterworth band-pass filter for the symmetric and asymmetric mode at a generator frequency of 275 kHz in the 90° direction

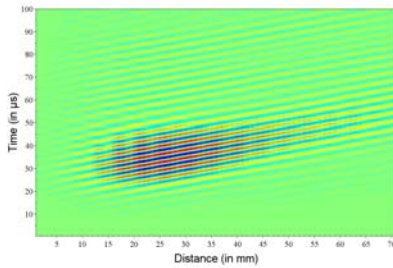


Figure 16: 2D plot of signal amplitude (in mV) of S_0 mode over time (in μs) and distance (in mm) at a generator frequency of 275 kHz in the 90° direction.

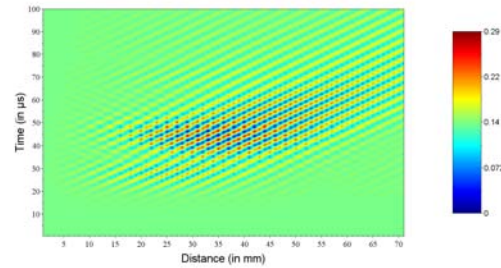


Figure 17: 2D plot of signal amplitude (in mV) of A_0 mode over time (in μs) and distance (in mm) at a generator frequency of 275 kHz in the 90° direction.

Another way to determine phase velocity is by measuring the time of arrival of a certain phase over distance. Here, the maximum of a wave mode was chosen and tracked over the whole distance, resulting in 70 points that can be described by a linear regression. The slope of the linear fit represents the phase velocity.

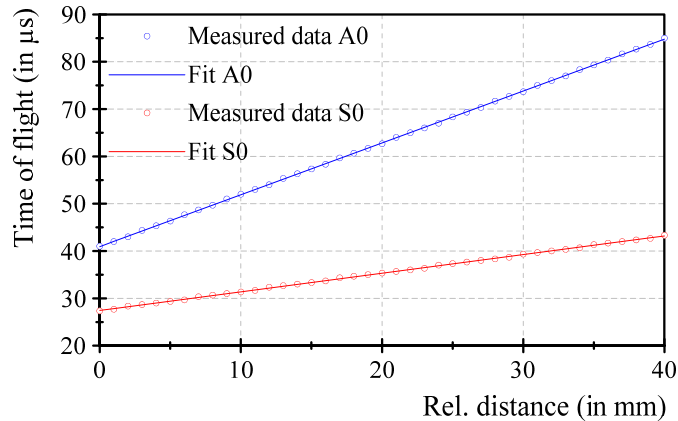


Figure 18: Time of flight (in μs) over relative distance (in mm) for A_0 (blue line) and S_0 (red line) mode at a generator frequency of 275 kHz in the 90° direction.

The results are shown in Table 3 which corresponds well with the approximated phase velocities from the peak coordinates of the 2D-FFT in Figure 15.

Parameter/Mode	A_0	S_0
Phase velocity (in m/s)	915	2530

Table 3: Phase velocities of A_0 and S_0 mode at a generator frequency of 275 kHz in the 90° direction. Results are obtained by tracking the time of arrival of the phase maximum.

Lamb wave attenuation can be determined by a similar approach. Instead of measuring the time of arrival, the amplitude of a certain phase is tracked over distance. Since the signal amplitude at the actuator is unknown, the amplitude A_1 (in mV) of the first measuring point at an actuator-sensor distance of x_1 (in mm; here: 30 mm) is chosen as a reference. For a point source excitation, the attenuation of lamb waves can be described as [16]:

$$\frac{A_2}{A_1} = \frac{\sqrt{x_1}}{\sqrt{x_2}} \cdot e^{-\alpha(x_2-x_1)} \quad (2)$$

where A_2 (in mV) is the amplitude of the signal at actuator-sensor distance x_2 (in mm) and α (1/mm) is the attenuation coefficient. This model considers attenuation via geometric spreading of the wave form (first term) as well as via intrinsic material damping (second term). By setting A_1 and x_1 as a reference and measuring A_2 over distance x_2 , the attenuation coefficient α can be determined by regression. Examples of wave attenuation for A_0 and S_0 are given in Figure 19 and Figure 20 for a generator frequency of 275 kHz in the 90° direction.

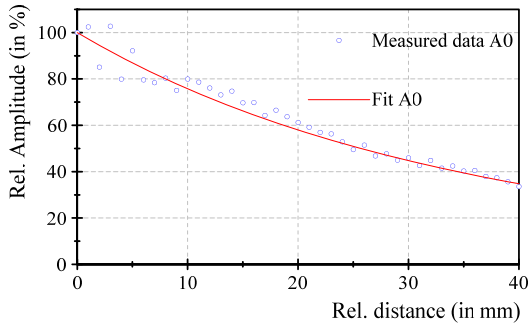


Figure 19: Signal amplitude (in %) of A_0 mode over relative distance (in mm) at a generator frequency of 275 kHz in the 90° direction.

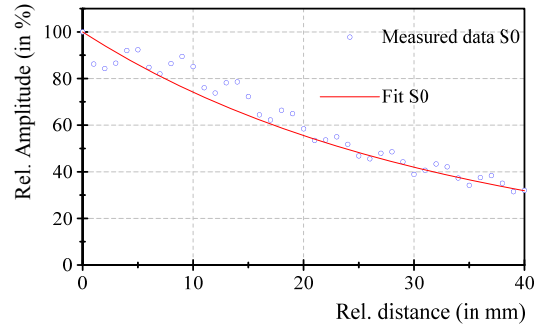


Figure 20: Signal amplitude (in %) of S_0 mode over relative distance (in mm) at a generator frequency of 275 kHz in the 90° direction.

As can be seen from the fit (red line), the measured data and the underlying model are in good agreement. The resulting attenuation factors are presented in Table 4.

Parameter/Mode	A_0	S_0
Attenuation factor α (in dB/mm)	0.13	0.28

Table 4: Attenuation factors of A_0 and S_0 mode at a generator frequency of 275 kHz in the 90° direction.

Following this approach, the respective phase velocities and attenuation coefficients of fundamental Lamb wave modes A_0 and S_0 can be determined independently as a function of fiber orientation for FRP laminates in the specified frequency range.

4 CONCLUSIONS

This study was focused on two types of smart structures: structures with integrated SMA wires for the realization of shape control and structures with integrated piezoelectric transducers for the realization of a guided wave SHM system. New concepts for the manufacturing of these structures were introduced along with a discussion about the major challenges. With a closer look taken at the interaction of system components, approaches for the characterization of smart structures were presented.

The approach using semi-finished SMA grids for the integration in FRP enables an improved load transfer by mechanical interlocking, the generation of an electrical network and an improved reproducibility at once.

An application-related characterization of the SMA actuation working against a stiffness delivers a comprehensive data base, mapping the whole interaction between counterpart behavior and shape memory effect actuation.

For the realization of a guided wave SHM system, a manufacturing method for the reproducible integration of piezoelectric transducers into fiber reinforced plastics during the RTM process was presented. The method allows for the integration of the active element within the original manufacturing process, omitting time consuming and sensitive post-processes.

Regarding the characterization, a method for the evaluation of Lamb wave attenuation and dispersion was suggested. The method facilitates the separation of symmetric and asymmetric mode by the application of a 2D-FFT along with a band-pass filter in time and space. Following this approach, exemplary values for phase velocities and attenuation factors for CFRP perpendicular to the fiber direction were determined.

REFERENCES

- [1] H. Janocha, *Adaptronics and Smart Structures – Basics, Materials, Design and Applications*. Springer, New York, 2007.
- [2] G. Marsh, *Airbus takes on Boeing with composite A350 XWB*. www.reinforcedplastics.com/view/1106/airbus-takes-on-boeing-with-compositea350-xwb/, (3/22/2012).
- [3] W. Huang, On the selection of shape memory alloys for actuators. *Materials and Design*, **23**, 11–9, 2002.
- [4] D.C. Lagoudas, *Shape Memory Alloys*. Springer, New York, 2008.
- [5] A. Czechowicz, J. Böttcher, S. Mojrzisch, S. Langbein, Speed shape memory alloy activation. *Proceedings of ASME Conference on Smart Materials, Adaptive Structures and Intelligent Systems*, Stone Mountain (Georgia, USA), 2012.
- [6] J.A. Balta, V. Michaud, J.-A. E. Månson, Adaptive Composite Materials Processing. *Proceedings of European Conference on Composite Materials*, Brugge (Belgium), 2010.
- [7] F. Daghia, G. Faiella, V. Antonucci, M. Giordano, Thermomechanical Modelling and Experimental Testing of a Shape Memory Alloy Hybrid Composite Plate. *Advances in Science and Technology*, **59**, 41–46, 2008.
- [8] E. L. Kirkby, J. O’Keane, R. de Oliveira, V. J. Michaud, J.-A. E. Månson, Tailored processing of epoxy with embedded shape memory alloy wires. *Smart Materials and Structures*, **18**, 095043, 2009.
- [9] T. L. Turner, C. L. Lach, R. J. Cano, Fabrication and characterization of SMA hybrid composites. *8th International Symposium on Smart Structures and Materials*, Newport Beach (California, USA), 2001.
- [10] K. Diamanti, C. Soutis, Structural health monitoring techniques for aircraft composite structures. *Progress in Aerospace Sciences*, **46**, 342-352, 2010.
- [11] Z. Su, L. Ye, Y. Lu, Guided Lamb waves for identification of damage in composite structures: A review. *Journal of Sound and Vibration*, **295**, 753-780, 2006.
- [12] Y. Wang, L. Zhou, Z. Wang, H. Huang, L. Ye, Analysis of internal stresses induced

by strain recovery in a single SMA fiber–matrix composite. *Composites Part B*, **42**, 1135-1143, 2011.

- [13] K. Potter, *Resin Transfer Moulding*. Springer, London, 1997.
- [14] M. Hübler, M. Gurka, U. P. Breuer, From attached shape memory alloy wires to integrated active elements, a small step? Impact of local effects on direct integration in fiber reinforced plastics. *Journal of Composite Materials*, **0**, 1-11, 2014.
- [15] D. N. Alleyne, *The non destructive testing of plates using ultrasonic lamb waves*. Imperial College of Science, Technology and Medicine, London, 1991.
- [16] M. Calomfirescu, *Lamb waves for structural health monitoring in viscoelastic composite materials*. Logos, Berlin, 2008